Performance Evaluation of a 100-W Class Hall Thruster

IEPC-2019-447

Presented at the 36th International Electric Propulsion Conference
University of Vienna • Vienna, Austria
September 15-20, 2019

Hiroki Watanabe[1]
Tokyo Metropolitan University, Hino, Tokyo, 191-0065, Japan

Shinatora Cho[2]
Japan Aerospace Exploration Agency, Sagamihara, Kanagawa, 252-5210, Japan

and

Kenichi Kubota[3]
Japan Aerospace Exploration Agency, Chofu, Tokyo, 182-8522, Japan

Abstract: A 100 W class Hall thruster with inner and outer electromagnetic coils was developed, and its discharge and plume characteristics were experimentally evaluated. The 100-W Hall thruster required a maximum magnetic flux density along the channel centerline above 24.3 mT to achieve efficient operation above a discharge voltage of 225 V and to achieve stable operation above a discharge voltage of 275 V. As typical thrust performance, an anode specific impulse of 1,050 s, thrust-to-discharge-power ratio of 59.5 mN/kW, and anode efficiency of 0.306 were achieved at a discharge voltage of 225 V and a discharge power of 88.9 W under a background pressure of 7.9×10^{-4} Pa. The plasma plume profile was measured using a nude-type Faraday probe, Langmuir probe, E×B probe, and retarding potential analyzer. The measured plume profile demonstrated that the low anode efficiency of the 100-W Hall thruster was due to low propellant utilization and large ion beam divergence.

Nomenclature

B	=	maximum radial magnetic flux density on discharge channel centerline
e	=	elementary charge
F	=	thrust
I_a	=	axial ion beam current
I_b	=	total ion beam current
I_d	=	discharge current
$\overline{I_d}$	=	average discharge current
J_b	=	ion beam current density
$\dot{m}_a$	=	anode mass flow rate
m_{xe}	=	mass of a xenon atom
r	=	radial distance from thruster centerline
V_d	=	discharge voltage
V_{mp}	=	most probable ion potential
V_p	=	plasma potential in plume

[1] Assistant Professor, Department of Aeronautics and Astronautics, hwatanabe@tmu.ac.jp.
[2] Researcher, Research and Development Directorate, choh.shinatora@jaxa.jp.
[3] Researcher, Aeronautical Technology Directorate, kubota.kenichi@jaxa.jp.

y_0	=	ratio of neutral speed to singly-charge ion speed
Z_i	=	charge-state of the *i*th ion species
Δ	=	amplitude of discharge current oscillation
η_a	=	anode efficiency
η_b	=	beam efficiency
η_c	=	current utilization efficiency
η_m	=	mass utilization efficiency
η_n	=	neutral-gain utilization efficiency
η_q	=	charge utilization efficiency
η_v	=	voltage utilization efficiency
Ω_i	=	current fractions of the *i*th ion species
τ	=	measurement time
ψ	=	effective plume divergence half-angle

I.Introduction

HALL thrusters with an input power of several hundred watts have received grate attention as the primary thrusters for micro and small satellites[1]. However, Hall thrusters with a nominal discharge power of 100 W or less[2-4] have exhibited low thrust performance compared to middle- and high-power Hall thrusters. The increase in the surface-to-volume ratio owing to the thruster downsizing is essentially the cause for the low thrust performance in low-power Hall thrusters. Moreover, the small inner channel diameter makes it difficult to design an optimal magnetic field topology. Cylindrical Hall thrusters[5-6] have been developed as a unique idea to avoid the increase in the surface-to-volume ratio; however, their thrust performance is still comparable to the thrust performance of the low-power annular-type Hall thrusters.

The high surface-to-volume ratio and difficulty in magnetic circuit design are challenging issues when attempting to achieve efficient operation in 100 W class Hall thrusters. In the present study, we developed a 100 W class Hall thruster with inner and outer electromagnetic coils. The discharge and plume characteristics of the 100-W Hall thruster were evaluated as a function of the magnetic field strength and discharge voltage in order to discuss the magnetic field requirement and performance improvement of low-power Hall thrusters.

II.Experimental Apparatus and Procedure

A. 100-W Class Hall Thruster

Figure 1 shows a cross-section diagram and magnetic field profile of the 100-W Hall thruster head. The discharge channel and anode are composed of boron nitride and molybdenum, respectively. The discharge channel of the 100-W Hall thruster was fabricated with a mean diameter of 20 mm and a width of 6 mm. The distance from the anode downstream surface to the channel exit plane was 8 mm. A commercial plasma bridge cathode with tungsten wire[7] was externally mounted.

The relationship between the channel exit position and the magnetic field topology was the typical configuration of a modern Hall thruster[8]. The thruster was composed of inner and outer concentric coils that were responsible for

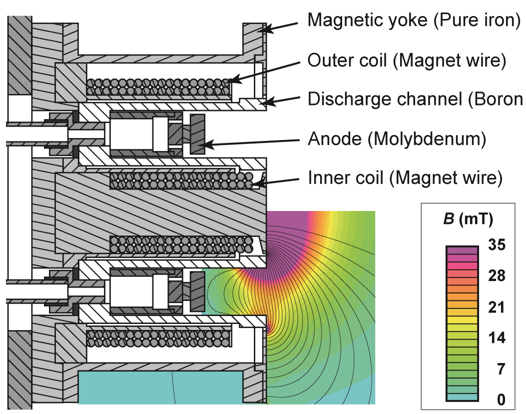

Figure 1. Cross-section diagram and magnetic field profile of 100-W Hall thruster. The magnetic profile was obtained by using magnetic simulation tool "FEMM."

inducing the magnetic field. The channel exit plane was near the magnetic flux density peak along the channel centerline, as shown in Fig. 1. The magnetic flux density near the anode was kept significantly low by using inner and outer screen yokes. Because of the thermal limit of the coil wire, the magnetic circuit could induce a maximum radial magnetic flux density along the channel centerline of up to 24.3 mT.

B. Vacuum Facility

A performance test was conducted in the Large Space Science Chamber located at the Institute of Space and Astronautical Science. The vacuum facility and experimental setup are schematically shown in Fig. 2. The vacuum chamber diameter and length were 2.5 m and 5.0 m, respectively. Two cryogenic pumps and one turbomolecular pump were installed in the chamber to provide a 24 kL/s pumping speed of xenon. The background pressure was measured by an ionization gauge attached to the vacuum chamber wall near the thruster. The base pressure (no-gas load) was 3.4×10^{-5} Pa.

C. Power Supplies and Propellant Feed System for Thruster Operation

DC power supplies for the thruster operation were connected to the thruster from outside the chamber. The electric circuit diagram of the thruster operation is shown in Fig. 3. The output terminals of the power supplies were isolated from the ground potential. The vacuum chamber and beam dump were grounded. The inner and outer electromagnetic coils were connected to each power supply to change the magnetic field strength while maintaining the magnetic field

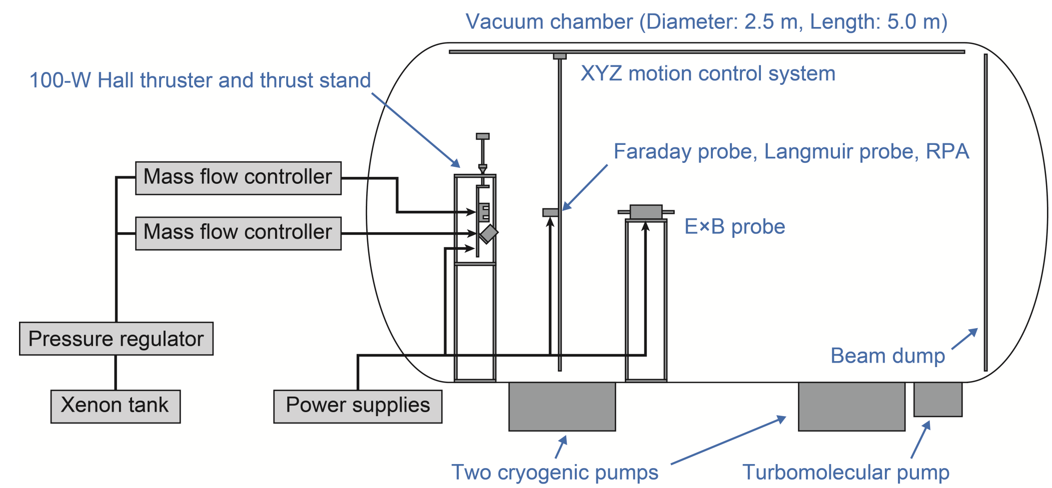

Figure 2. Vacuum facility and experimental setup (not on scale).

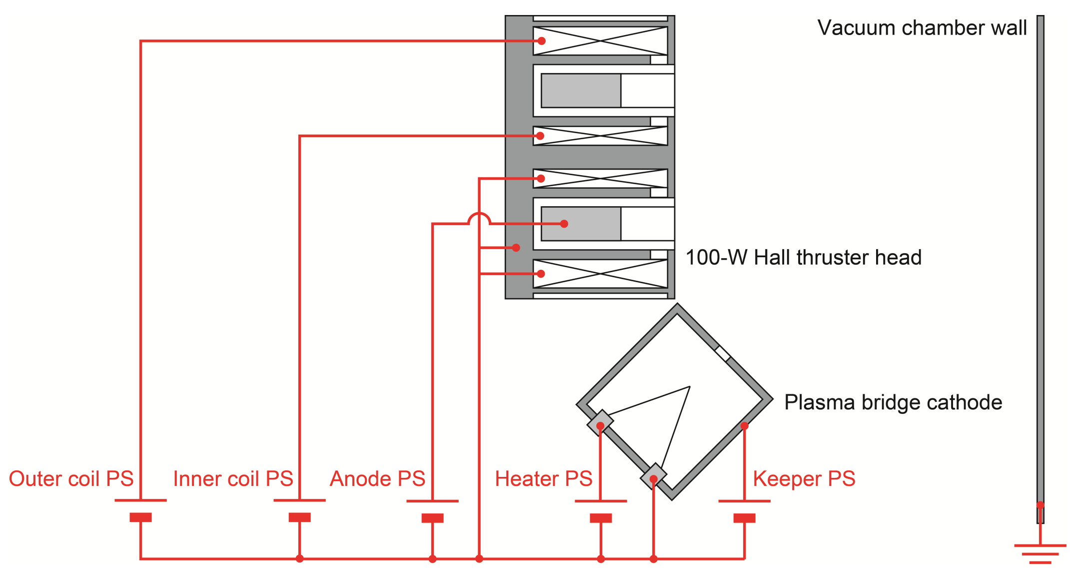

Figure 3. Circuit diagram of Hall thruster operation. "PS" is power supply.

Table 1. Anode mass flow rate and background pressure for various discharge voltages. Because the ionization gauge was calibrated for nitrogen, the background pressure was corrected for xenon using the gas correction factor.

Discharge voltage, V	Anode mass flow rate, mg/s	Background pressure, Pa
150	0.655	9.8×10^{-4}
175	0.616	9.3×10^{-4}
200	0.547	8.4×10^{-4}
225	0.513	7.9×10^{-4}
250	0.454	7.1×10^{-4}
275	0.410	5.9×10^{-4}
300	0.376	5.4×10^{-4}

topology. The thruster body and the negative terminal of the coil power supplies were tied to cathode common.

Xenon propellant was fed to the anode and cathode via mass flow controllers. The cathode flow rate was maintained at 10% of the anode mass flow rate. To evaluate the thrust performance at a constant discharge power, the anode mass flow rate for various discharge voltages was selected to have a discharge power of approximately 85 W under the magnetic field strength at which the anode efficiency is maximum. Table 1 lists the anode mass flow rates and background pressures for various discharge voltages.

D. Instrumentation

The thrust was measured using a pendulum-type thrust stand with an optical displacement sensor. The stand was calibrated using measured masses on a pulley system connected to a stepping motor stage. To minimize the measurement error owing to thermal drift, the thrust stand's zero was measured for each thrust measurement.

The discharge current and its oscillation were measured using a current probe. The amplitude of the discharge current oscillation, Δ, is defined as follow[9]:

$$\Delta=\frac{1}{\overline{I}_\mathrm{d}}\sqrt{\frac{\int_0^\tau (I_\mathrm{d}-\overline{I}_\mathrm{d})^2 dt}{\tau}}, \tag{1}$$

where I_d, τ, and $\overline{I}_\mathrm{d}$ are the discharge current, measurement time, and average discharge current.

The plume was measured using a nude-type Faraday probe, Langmuir probe, E×B probe, and retarding potential analyzer (RPA). The E×B probe was located 1 m downstream of the channel exit plane. The Faraday probe, Langmuir probe, and RPA were placed on an XYZ motion control system. The center of the Langmuir probe, E×B probe, and RPA was positioned on the discharge channel centerline.

E. Hall Thruster Performance Architecture

To evaluate the Hall thruster performance, the anode efficiency, η_a, is defined as follow:

$$\eta_\mathrm{a}=\frac{F^2}{2\dot{m}_\mathrm{a}\overline{I}_\mathrm{d}V_\mathrm{d}}=\eta_\mathrm{v}\eta_\mathrm{c}\eta_\mathrm{q}\eta_\mathrm{m}\eta_\mathrm{n}\eta_\mathrm{b}, \tag{2}$$

where F, $\dot{m}_\mathrm{a}$, and V_d are the thrust, anode mass flow rate, and discharge voltage, respectively. The anode efficiency describes the jet power divided by the discharge power and anode flow rate. Based on the methodology of a Hall thruster efficiency analysis developed by Brown et al.[10], the anode efficiency is the product of six Hall thruster efficiencies: voltage utilization, η_v, current utilization, η_c, charge utilization, η_q, mass utilization, η_m, neutral-gain utilization, η_n, and beam, η_b. The efficiencies are defined as follows:

$$\eta_\mathrm{v}=\frac{V_\mathrm{mp}-V_\mathrm{p}}{V_\mathrm{d}}, \tag{3}$$

$$\eta_\mathrm{c}=\frac{I_\mathrm{b}}{\overline{I}_\mathrm{d}}, \tag{4}$$

$$\eta_\mathrm{q}=\frac{\left[\sum\left(\Omega_\mathrm{i}/\sqrt{Z_\mathrm{i}}\right)\right]^2}{\sum\left(\Omega_\mathrm{i}/Z_\mathrm{i}\right)}, \tag{5}$$

$$\eta_\mathrm{m}=\frac{m_\mathrm{xe}I_\mathrm{b}}{e\dot{m}_\mathrm{a}}\sum\frac{\Omega_\mathrm{i}}{Z_\mathrm{i}}, \tag{6}$$

$$\eta_\mathrm{n}=1+2y_0\frac{1-\eta_\mathrm{m}}{\eta_\mathrm{m}\sqrt{\eta_\mathrm{q}/\sum\left(\Omega_\mathrm{i}/Z_\mathrm{i}\right)}}, \tag{7}$$

$$\eta_b = \left(\frac{I_a}{I_b}\right)^2, \tag{8}$$

where V_{mp}, V_p, I_b, Ω_i, Z_i, m_{xe}, e, y_0, and I_a are the most probable ion potential, plasma potential, total ion beam current, current fractions of the ith ion species, charge-state of the ith ion species, mass of a xenon atom, elementary charge, ratio of the neutral speed to the singly charged ion speed, and axial ion beam current, respectively. From the measured ion[13] and neutral[14] velocity at discharge voltages ranging from 150 to 250 V, the value of y_0 was assumed to be 0.02.

III.Experimental Results and Discussion

A. Discharge Characteristics

Figures 4 and 5 show the average discharge current and amplitude of discharge current oscillation as a function of the magnetic field strength for various discharge voltages. The average discharge current decreased as the magnetic field increased. In addition, the average discharge current remained constant at higher magnetic field strength except a discharge voltage of 150 V. For discharge voltages ranging from 150 to 200 V, a discharge current oscillation was suppressed at higher magnetic field strengths. On the other hand, above a discharge voltage of 200 V, a discharge current oscillation was induced at magnetic flux densities ranging from 14.8 to 20.8 mT. The discharge current oscillation was suppressed at 24.3 mT except 300 V. Moreover, the magnetic field strength required to suppress the oscillation increased as the discharge voltage increased. To suppress the breathing-mode oscillation, Yamamoto et al.[9] demonstrated that the electron flow to the ionization region should be restricted. The axial electron velocity increased

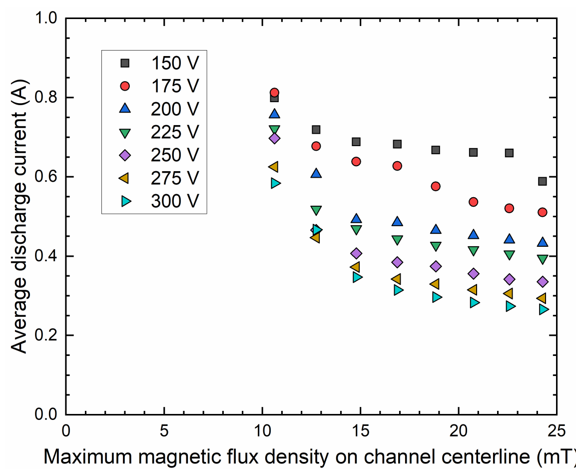

Figure 4. Average discharge current as a function of magnetic field strength for various discharge voltages.

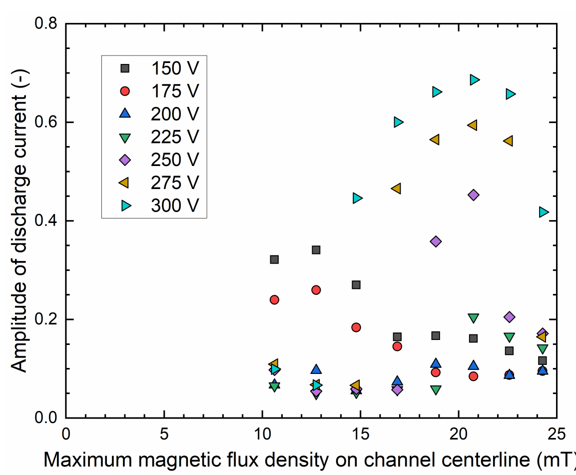

Figure 5. Amplitude of discharge current oscillation as a function of magnetic field strength for various discharge voltages.

as the discharge voltage increased. Thus, when the discharge voltage increases, the magnetic field strength increases to restrict the inflow. The relationship between the magnetic field strength and discharge voltage resulted in an increase in the magnetic field strength, as shown in Fig. 5. Therefore, the magnetic field strength was not sufficiently high to suppress the current oscillation at a discharge voltage of 300 V.

Figures 6 and 7 show the thrust and anode efficiency as a function of the magnetic field strength for various discharge voltages. The anode efficiency shown in Fig. 7 was calculated using Eq. (2) by the thrust and average discharge current. The thrust increased as the magnetic field was strengthened. Above 200 V, the thrust decreased when the current oscillation was induced, and then increased as the oscillation became weak. As a result, the current oscillation degraded the thrust performance of the 100-W Hall thruster. For discharge voltages ranging from 175 to 225 V, the anode efficiency saturated at over 22.6 mT. However, above 225 V, the anode efficiency did not saturate at 24.3 mT. The data presented in Figs. 4-7 demonstrated that the magnetic field strength of the 100-W Hall thruster was not sufficiently high to achieve efficient operation above 225 V.

Figure 8 shows the thrust performance for various discharge voltages under the magnetic field strength at which the anode efficiency is maximum. The cathode mass flow rate was excluded from the calculation of the specific impulse. In addition, the power consumption of the electromagnetic coils and plasma bridge cathode were excluded from the calculation of the thrust-to-power ratio. For discharge voltages ranging from 150 to 250 V, the anode efficiency improved as the discharge voltage increased. Above 250 V, the specific impulse remained constant in spite of the increase in discharge voltage and the anode efficiency degraded, because the magnetic field was not sufficiently high to achieve efficient operation. Hence, as typical thrust performance, a specific impulse of 1,050 s, thrust-to-power ratio of 59.5 mN/kW, and anode efficiency of 0.306 were achieved at a discharge voltage of 225 V and a discharge power of 88.9 W.

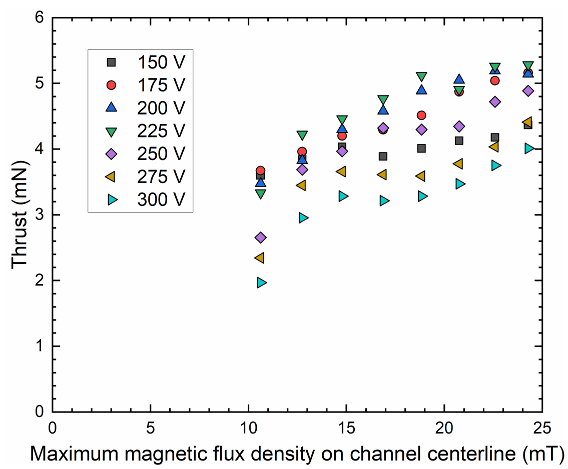

Figure 6. Thrust as a function of magnetic field strength for various discharge voltages.

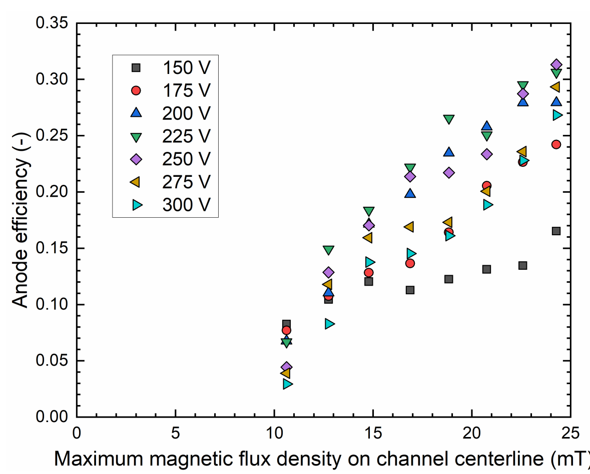

Figure 7. Anode efficiency as a function of magnetic field strength for various discharge voltages.

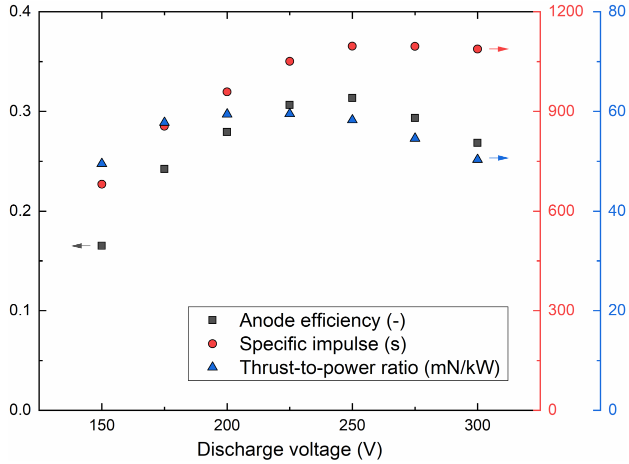

Figure 8. Thrust performance for various discharge voltages under magnetic field strength at which anode efficiency is maximum.

B. Plume Characteristics

1. Most Probable Ion Potential

Figure 9 shows the typical RPA trace and analysis technique. The most probable ion potential was determined by dI/dV in the RPA trace. Figure 10 shows the most probable ion potential as a function of the magnetic field strength for various discharge voltages. The most probable ion potential was obtained at 500 mm downstream of the channel exit plane. At 200 and 225 V, the most probable ion potential slightly fell as the magnetic flux density increased. The sharp fall in the most probable ion potential was detected at 275 V when the discharge current oscillation was induced. Moreover, the most probable ion potential rose when the oscillation was suppressed at 24.3 mT.

2. Plasma Potential in Plume

Figure 11 shows the typical Langmuir probe trace and analysis technique. The plasma potential of the plume was determined by curve fitting of the "knee" in the Langmuir probe trace. Figure 12 shows the plasma potential as a function of the magnetic field strength for various discharge voltages. The plasma potential was also obtained at 500 mm downstream of the channel exit plane. The plasma potential did not depend on the discharge voltage. Above a magnetic flux density of 14.8 mT, the plasma potential slightly rose with the increasing of the magnetic field strength. Moreover, the variation in the plasma potential owing to the change in the magnetic field strength was small.

3. Current Fractions of ith Ion Species

Figure 13 shows typical E×B probe trace and analysis technique. The method of Gaussian fitting[11] was applied to the analysis of the E×B probe trace to obtain the current fractions of the *i*th ion species. Figure 14 shows the current fractions of the *i*th ion species as a function of the magnetic field strength for various discharge voltages. The effect of the magnetic field strength on the production of multiply charged ions was minimal at 200 and 225 V. However, the discharge current oscillation affected the multiply charged ion production at 275 V.

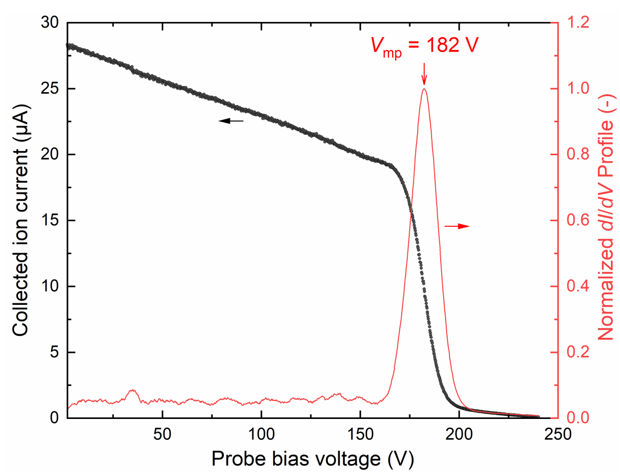

Figure 9. Typical RPA trace and analysis technique: V_d = 200 V and B =24.3 mT.

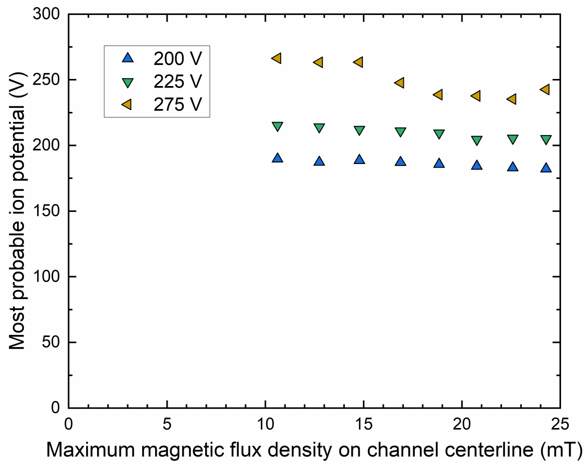

Figure 10. Most probable ion potential as a function of magnetic field strength for various discharge voltages.

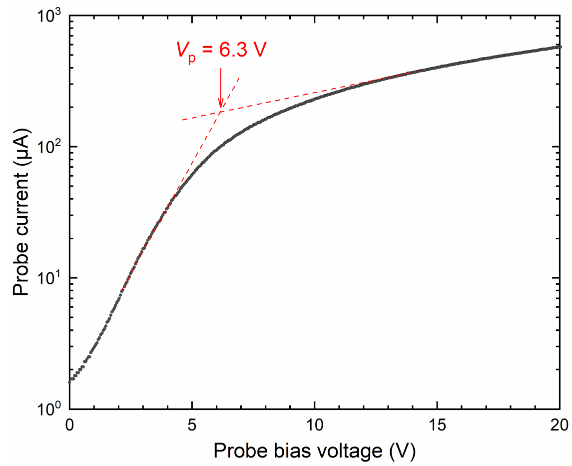

Fig. 11 Typical Langmuir probe trace and analysis technique: V_d = 200 V and B =24.3 mT.

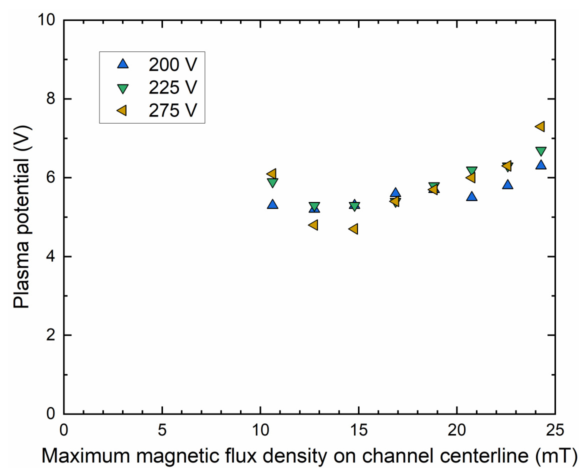

Figure 12. Plasma potential in plume as a function of magnetic field strength for various discharge voltages.

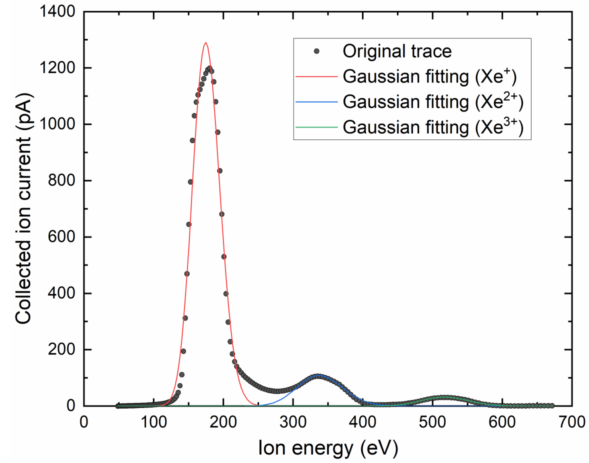

Figure 13. Typical E×B probe trace and analysis technique: V_d = 200 V and B =24.3 mT.

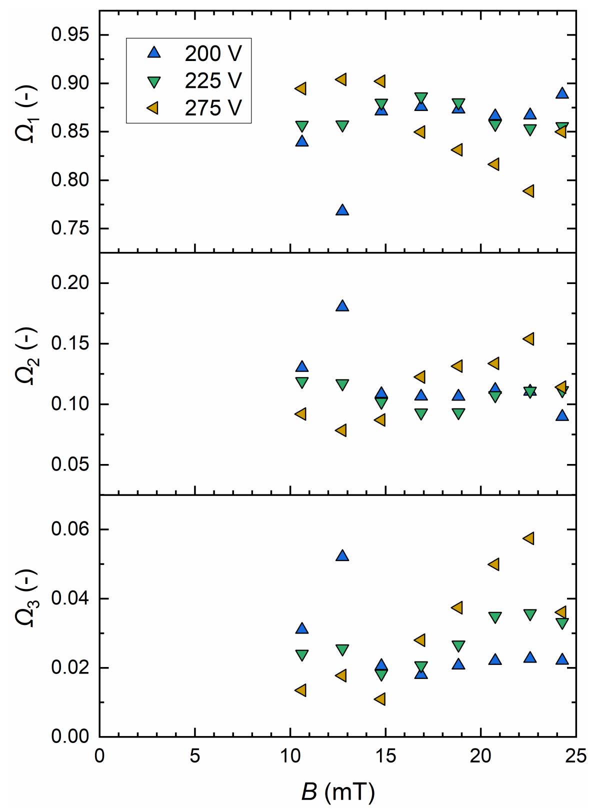

Figure 14. Current fractions of the *i*th ion species as a function of magnetic field strength for various discharge voltages.

4. Ion Beam Current and Divergence

Figure 15 shows the typical Faraday probe trace. By using the Faraday probe trace, the total ion beam current and axial ion beam current were calculated for an axisymmetric plume about the thruster centerline in Eqs. (9) and (10).

$$I_b = 2\pi \int_0^{450} r J_b(r) dr, \tag{9}$$

$$I_a = 2\pi \int_0^{450} r J_b(r) \cos\theta dr, \tag{10}$$

where r, $J_b(r)$, and θ are the radial distance from the thruster centerline, radial distribution of the ion current density, and probe angle, respectively. A correction for secondary electron emission at the molybdenum collector surface[12]

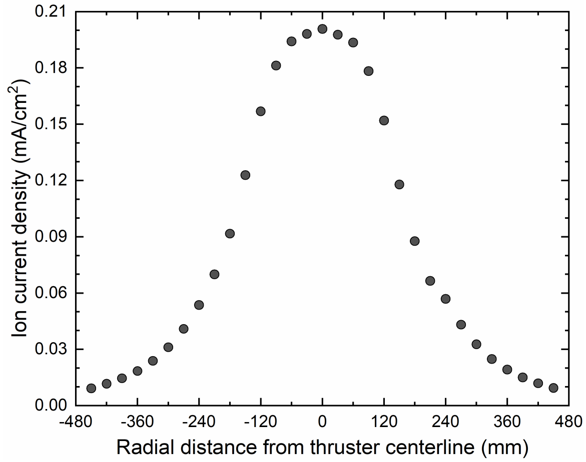

Figure 15. Typical Faraday probe trace and analysis technique: V_d = 200 V and B =24.3 mT.

was applied to the ion current density measurement. In Eqs. (9) and (10), the measured current densities from each side of the plume (0 mm to 450 mm and 0 mm to -450 mm) are integrated, and the calculated beam currents are the average of the two sides. The effective plume divergence half-angle was defined as follow:

$$\psi = \cos^{-1}\left(\frac{I_a}{I_b}\right). \tag{11}$$

Figures 16 and 17 show the total ion beam current and the effective plume divergence half-angle as a function of the magnetic field strength for various discharge voltages. The ion beam current was obtained at 300 mm downstream of the channel exit plane. Regardless of the discharge voltage, the total ion beam current increased as the magnetic field strength increased, as shown in Fig. 16. However, the total ion beam current decreased at 225 V when the discharge current oscillation was induced at 20.8 mT. Moreover, the total ion beam current sharply increased at 275 V when the discharge current oscillation was suppressed. The increase in the magnetic field strength enhanced the ion beam focusing, as shown in Fig. 17. However, the ion beam diverged at 225 V when the discharge current oscillation was induced. At 24.3 mT, the ion beam focused as the discharge voltage increased.

5. Loss Evaluation

Figure 18 shows the Hall thruster efficiencies as a function of magnetic field strength at a discharge voltage of 225 V. The effect of the magnetic field strength on the charge efficiency was minimal, and the neutral-gain utilization efficiency decreased slightly as the magnetic field strength increased. The current utilization, mass utilization, and beam efficiencies improved as the magnetic field strength increased and then saturated at higher magnetic field strengths, whereas the voltage utilization decreased slightly as the magnetic field strength increased. However, the current utilization, mass utilization, and beam efficiencies decreased when the discharge current oscillation was induced at 20.8 mT and increased as the oscillation became weak. In addition, the voltage utilization sharply decreased

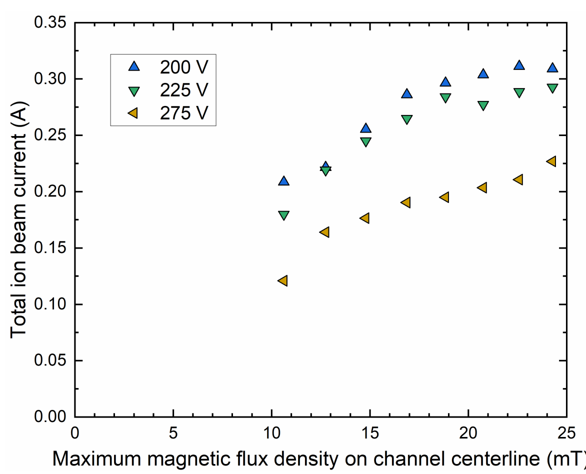

Figure 16. Total ion beam current as a function of magnetic field strength for various discharge voltages.

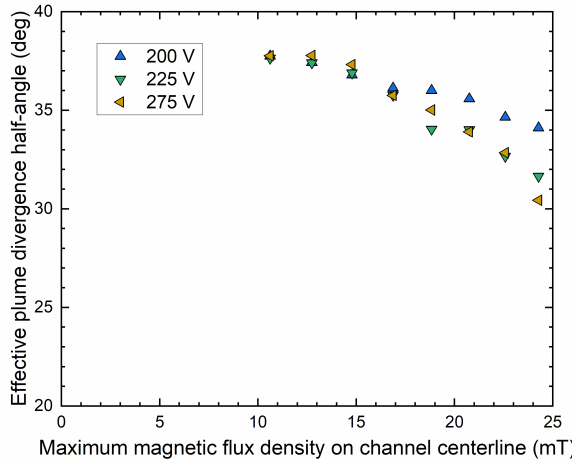

Figure 17. Effective plume divergence half-angle as a function of magnetic field strength for various discharge voltages.

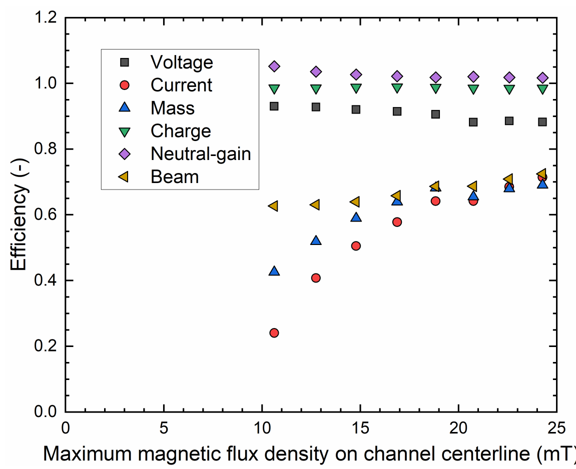

Figure 18. Hall thruster efficiencies as a function of magnetic field strength at a discharge voltage of 225 V.

when the discharge current oscillation was induced.

Figure 19 shows the anode efficiency as a function of magnetic field strength at a discharge voltage of 225 V. In Fig. 19, red circle and black square symbols indicate the anode efficiency calculated using Eq. (2) by the plasma plume property and by the thrust and discharge current, respectively. The anode efficiency predicted by the thrust and discharge current corresponded to that predicted by the plume profile. In addition, the degradation of the anode efficiency at 20.8 mT was detected by using the plume profile. The degradation was caused by the thrust change, as shown in Fig. 6. The plume profile presented in Fig. 18 indicates that thrust change was caused by changes in propellant utilization, electron confinement by the magnetic field, and beam divergence. These results demonstrated that the measured plume profile and predicted efficiencies were validated and represented losses in the performance of the 100-W Hall thruster. Consequently, the low anode efficiency of the 100-W Hall thruster was mainly due to the degradation in the mass utilization and beam efficiencies, as shown in Fig. 18. Hence, low propellant utilization and a large beam divergence are critical issues for achieving efficient operation in Hall thrusters with a nominal discharge power of 100 W or less.

IV.Conclusion

The 100-W Hall thruster with inner and outer electromagnetic coils was developed to discuss the magnetic field requirement and performance improvement of low-power Hall thrusters. The discharge and plume characteristics of the 100-W Hall thruster were experimentally evaluated by using the thrust stand, nude-type Faraday probe, Langmuir probe, E×B probe, and RPA.

The 100-W Hall thruster required a maximum magnetic flux density along the channel centerline above 24.3 mT

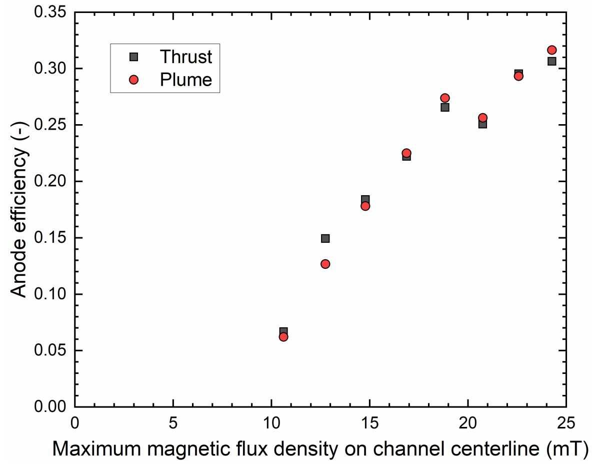

Figure 19. Anode efficiency as a function of magnetic field strength at a discharge voltage of 225 V.

to achieve efficient operation above a discharge voltage of 225 V and to achieve stable operation above a discharge voltage of 275 V. Hence, as typical thrust performance, a specific impulse of 1,050 s, thrust-to-power ratio of 59.5 mN/kW, and anode efficiency of 0.306 were achieved at a discharge voltage of 225 V and a discharge power of 88.9 W under a background pressure of 7.9×10^{-4} Pa.

The measured plume profile and predicted Hall thruster efficiencies were validated, because the anode efficiency predicted by the thrust and discharge current corresponded to that predicted by the plume profile. From the plume plasma profile, the low anode efficiency of the 100-W Hall thruster was mainly due to the degradation in the mass utilization and beam efficiencies. Therefore, low propellant utilization and a large beam divergence are critical issues for achieving efficient operation in Hall thrusters with a nominal discharge power of 100 W or less.

Acknowledgments

This research results were obtained using Space Chamber Laboratory of ISAS, JAXA. This study was supported by JSPS KAKENHI Grand Number 17H04972.

References

[1]Lev, D., Myers, R., Lemmer, K., Kolbeck, J., Koizumi, H., Polzin, L, "The Technological and Commercial Expansion of Electric Propulsion," *Acta Astronautica*, Vol. 159, No. 6, pp. 213-227, 2019.

[2]Mazouffre, S., Grimaud, L., "Characteristics and Performances of a 100-W Hall Thruster for Microspacecraft," *IEEE Transactions on Plasma Science*, Vol. 46, No.2, pp. 330-337, 2018.

[3]Szabo, J. Tedrake, R., Metivier, E., Paintal, S., Taillefer, X., "Characterization of a One Hundred Watt, Long Lifetime Hall Effect Thruster for Small Spacecraft," *Proceedings of 53rd AIAA/SAE/ASEE Joint Propulsion Conference*, AIAA 2017-4728, 2017.

[4]Loyan, A., Maksymenko, T., "Performance Investigation of SPT-20M Low Power Hall Effect Thruster," *Proceedings of 30th International Electric Propulsion Conference*, IEPC 2007-100, 2007.

[5]Sminov, A., Ratses, Y., Fisch, N., "Experimental and Theoretical Studies of Cylindrical Hall Thrusters," *Physics of Plasmas*, Vol. 14, No. 5, 057106, 2007.

[6]Ikeda, T., Togawa, K., Tahara, H., Watanabe, Y., "Performance Characteristics of Very Low Power Cylindrical Hall Thrusters for the Nano-Satellite "PROITERES-3"," *Vacuum*, Vol. 88, No. 2, pp.63-69, 2013.

[7]Reader, P., White, D., Isaacson, G., "Argon Plasma Bridge Neutralizer Operation with a 10-cm-beam-diameter Ion Etching Source," *Journal of Vacuum Science and Technology*, Vol. 15, No, 3, pp. 1093-1095, 1978.

[8]Kim, V, "Main Physical Features and Processes Determining the Performance of Stationary Plasma Thrusters," *Journal of Propulsion and Power*, Vol. 14, No. 5, pp. 736-743, 1998.

[9]Yamamoto, N., Komurasaki, K., Arakawa, Y., "Discharge Current Oscillation in Hall Thrusters," *Journal of Propulsion and Power*, Vol. 21, No. 5, pp. 870-876, 2005.

[10]Brown, D., Kaeson, W., Beal, B., Gallimore, A., "Methodology and Historical Perspective of a Hall Thruster Efficiency Analysis," *Journal of Propulsion and Power*, Vol. 25, No. 6, pp. 1163-1177, 2009.

[11]Shastry, R., Hofer, R., Reid, B., Gallimore, A., "Method for Analyzing E×B Probe Spectra from Hall Thruster Plumes," *Review of Scientific Instruments*, Vol. 80, No. 6, 063502, 2009.

[12]Brown, D. Walker, M., Szabo, J, Huang, W., Foster, J., "Recommended Practice for Use of Faraday Probes in Electric Propulsion Testing," *Journal of Propulsion and Power*, Vol. 33, No. 3, pp. 582-613, 2017.

[13]Hargus, W., Cappelli, M., "Interior and Exterior Laser-Induced Fluorescence and Plasma Measurements within a Hall Thruster," *Journal of Propulsion and Power*, Vol. 18, No. 1, 159-168, 2002.

[14]Huang, W., Gallimore, A., Hofer, R., "Neutral Flow Evolution in a Six-Kilowatt Hall Thruster," *Journal of Propulsion and Power*, Vol. 27, No. 3, 553-563, 2011.